Giant, 19, 2024, 100297

Full-length article

Biopolymer networks packed with microgels combine strain stiffening and shape programmability

Vignesh Subramaniam[a], Abhishek M. Shetty[b], Steven J. Chisolm[a], Taylor R. Lansberry[c], Anjana Balachandar[d], Cameron D. Morley[e], Thomas E. Angelini[a,c,f,*]

[a] University of Florida, Herbert Wertheim College of Engineering, Department of Mechanical and Aerospace Engineering, Gainesville, FL, 32611, USA
[b] Advanced Technical Center, Anton Paar USA, Ashland, VA, 23005, USA
[c] University of Florida, Herbert Wertheim College of Engineering, J. Crayton Pruitt Family Department of Biomedical Engineering, Gainesville, FL, 32611, USA
[d] Stanford University, Department of Bioengineering, Stanford, CA, 94305, USA
[e] University of California Berkeley, Department of Bioengineering, Berkeley, CA, 94720, USA
[f] University of Florida, Herbert Wertheim College of Engineering, Department of Materials Science and Engineering, Gainesville, FL, 32611, USA

Keywords: Biomaterials, Rheology, Reversible strain-stiffening, Shape programmability, Biopolymer non-linear elasticity, Microgel reconfigurability, Athermal rheological model of the cell

Biomaterials that can be reversibly stiffened and shaped could be useful in broad biomedical applications where form-fitting scaffolds are needed. Here we investigate the combination of strong non-linear elasticity in biopolymer networks with the reconfigurability of packed hydrogel particles within a composite biomaterial. By packing microgels into collagen-1 networks and characterizing their linear and non-linear material properties, we empirically determine a scaling relationship that describes the synergistic dependence of the material's linear elastic shear modulus on the concentration of both components. We perform high-strain rheological tests and find that the materials strain stiffen and also exhibit a form of programmability, where no applied stress is required to maintain stiffened states of deformation after large strains are applied. We demonstrate that this non-linear rheological behavior can be used to shape samples that do not spontaneously relax large-scale bends, holding their deformed shapes for days. Detailed analysis of the frequency-dependent rheology reveals an unexpected connection to the rheology of living cells, where models of soft glasses capture their low-frequency behaviors and polymer elasticity models capture their high-frequency behaviors.

1 Introduction

The material properties of biopolymer networks become highly non-linear in response to modest levels of applied strain, making them an appealing starting point for designing advanced materials having tunable and widely variable elasticity [7–10]. By contrast, networks made from flexible synthetic polymers typically exhibit negligible stiffening at the levels of applied strain where biopolymer networks are highly nonlinear [11,12]. Nonlinear material response is found in reconstituted extracellular matrix (ECM) networks like collagen and fibrin, and in reconstituted cytoskeletal networks like crosslinked F-actin [10,13–16]. Indeed, inspiration for tunable elastic materials can be drawn from

* Corresponding author.
E-mail address: t.e.angelini@ufl.edu (T.E. Angelini).
Received 31 January 2024; Received in revised form 21 May 2024; Accepted 25 May 2024

https://doi.org/10.1016/j.giant.2024.100297

the cell itself; the cytoskeleton exhibits soft-glassy rheological behavior [17–19], and its elasticity is controlled by cytoskeletal pre-stress generated by molecular motors like myosin [20–26]. However, making tunable elastic materials that rely on molecular motors involves challenges like the stability and spatial distribution of constituent proteins and transport limitations of their chemical fuel, adenosine triphosphate (ATP) [27,28]. To sidestep these limitations, it may be possible to leverage materials that do not spontaneously reverse states after a large strain is applied – packed soft granular materials. Previously, particles were incorporated into biopolymer networks to enhance their mechanical performance and mimic the compression-stiffening properties of certain biological tissues [29–34]. Additionally, micro-scale hydrogel particles (microgels) have been incorporated in biopolymer networks to make materials that stiffen in response to stimuli such as strain and temperature [35]. One of the most useful rheological properties of packed microgels is their ability to quickly relax stress after large strains have been imposed, in contrast to elastic networks that store elastic energy and work to return to states of zero strain. However, this property of microgels has not been leveraged in previous work on biopolymer-microgel composites. Combining the non-linear elasticity of biopolymers with the reconfigurability of microgels may enable the development of advanced materials that exhibit both tunable elasticity and shape programmability in response to mechanical stimulus.

Here, we investigate how packing microgels into strain-stiffening biopolymer networks leads to controllable and reversible material properties. We develop biocomposite materials made from collagen-1 networks filled with microgels made from polyethylene glycol (PEG). We find that combining collagen and microgels at relatively low concentrations produces materials with dramatically increased elastic shear moduli compared to the individual components. Additionally, non-linear rheological tests reveal that the composite materials "lock in" a finite strain after stress is applied and then removed, manifesting as a type of programmability in shape and elasticity; the reversibility of this effect represents a form of shape memory. Our analysis indicates that the collagen network provides the shape memory effect, while the packed microgels provide the programmability effect (Fig 1a-d). We demonstrate the shape-programmability and stability of these materials over the course of several days after imposing large deformations on molded structures. While previous studies of particle-ECM composites focused on material strength [30,33,34] and tissue-mimicking mechanical behaviors [31,32], the work described here uncovers potentially useful nonlinear properties that emerge synergistically from combining the two very different materials.

2 Results

To formulate the biopolymer-microgel composite materials we combine type-1 collagen solutions with PEG microgels, exploring a wide range of compositions. We synthesize the PEG microgels using an emulsion polymerization technique (Section 4.1) and suspend them in Phosphate-Buffered Saline (PBS) solution before mixing with solutions of molecular collagen. Using optical microscopy and digital image analysis, we find that the average microgel diameter is 9.46 ± 4.25 μm (Fig. S1). This diameter is within the same order of magnitude as the mesh size of a typical collagen network having a concentration of 1–3 mg/mL [36]. Testing the linear rheological responses of pure microgel samples at different packing densities, we find they become dominantly solid-like at a polymer concentration of 4.2 % (w/w), above which the elastic shear modulus, G', is larger than the viscous shear modulus, G'' (Fig. S2a). Thus, we formulate the microgel-biopolymer composite materials at PEG concentrations between 2 % and 6 % (w/w), spanning this threshold. We vary the collagen concentration over the range of 0.5 to 2 mg/mL. The samples are prepared using molecular collagen solutions; both the microgel and the collagen solutions are kept in an ice bath until they are mixed and brought to neutral pH. The sample temperature is ramped to 37^{0}C and cured for 45 min. An overlay

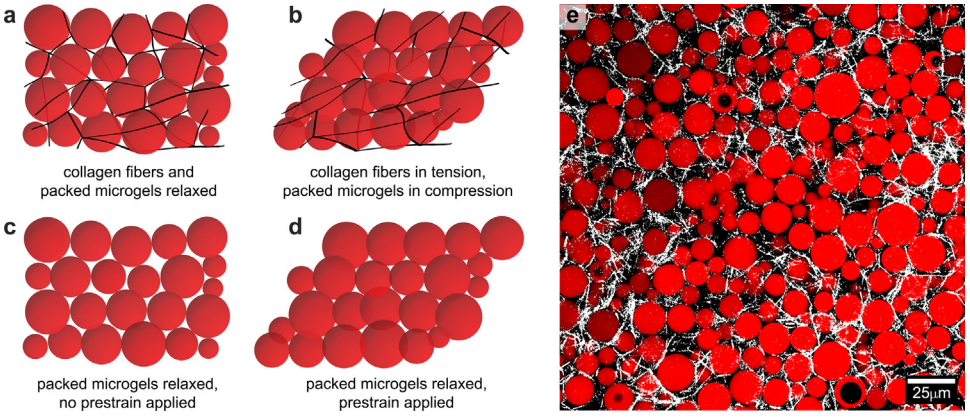

Fig. 1

Collagen-microgel composite material in strained and unstrained states. (a) Schematic of composite material with the collagen fibers and packed microgels in relaxed state. (b) Schematic of the composite material under shear strain where collagen fibers are in tension and packed microgels in compression. (c) Schematic of packed microgels in a relaxed state when no strain is applied on the material. (d) Schematic of packed microgels rearranged and in a relaxed state after shear strain is applied on the material. (e) An overlay of confocal fluorescence and reflectance micrographs of 4.7 % (w/w) packed microgels with an interpenetrating 1 mg/mL collagen fiber network.

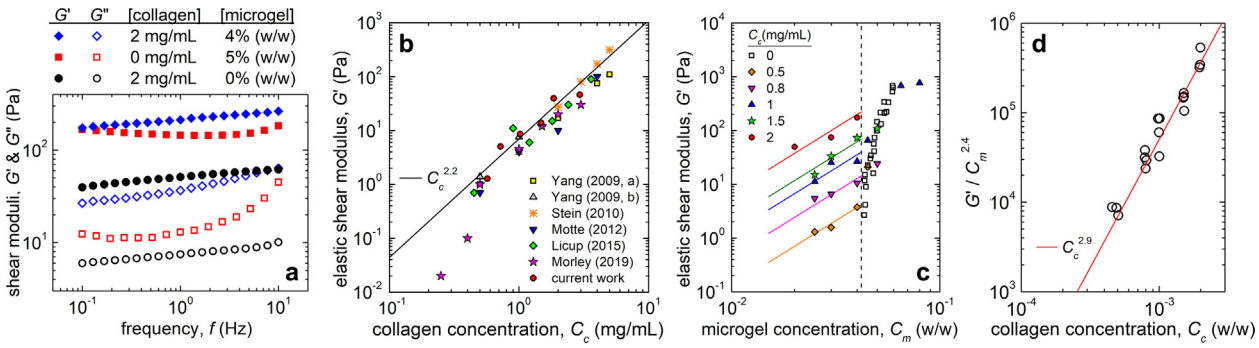

Fig. 2

Linear rheological characterization of collagen-microgel composite materials. (a) Elastic and viscous moduli of the composite materials show weak frequency dependence and an elastic solid-like behavior over a wide frequency range. The moduli of composite materials are larger than those of the individual components. (b) Elastic shear moduli of type-1 collagen gels at a representative oscillation frequency of 0.1 Hz overlaid on data from published literature[1–6] shows a scaling law of $G' \sim C_c^{2.2}$ above a collagen concentration of 0.4 mg/mL. (c) Collagen added to loosely packed microgels below a concentration of 4.2 % (w/w) dramatically increases the elastic modulus of the composite material. Free fitting power laws to the data at each collagen concentration reveals a scaling law of $G' \sim C_m^{2.4}$. (d) The power law analysis results in $G' / C_m^{2.4}$ collapsing at multiple collagen concentrations leading to a power law relation of $G' \sim C_c^{2.9}$ indicating a stronger scaling of elastic shear modulus with collagen concentration due to synergistic effects of the collagen-microgel composite materials.

of confocal fluorescence and reflectance micrographs shows the interpenetrating collagen network and packed microgels (Fig. 1e).

2.1 Mutual stiffening in the linear regime

The material properties of type-1 collagen networks strongly depend on the polymer concentrations. Prior work [1–6] has shown that $G' \sim C_c^{2.2}$, where G' is the elastic shear modulus and C_c is the collagen concentration. To check that our formulation method agrees with the published literature, we perform linear rheology on collagen gels. We measure shear moduli of the collagen gels using frequency sweeps and extract storage modulus, G', and loss modulus, G'', spanning a frequency range of 0.1 Hz to 10 Hz. Over this frequency range, we find that $G' > G''$ and both G' and G'' increase weakly with increasing frequency (Fig. 2a, S3). To test the scaling of G' with increasing collagen concentration, C_c, we choose a representative oscillation frequency of 0.1 Hz and overlay our G' data points on top of data from the published literature. We find that above $C_c = 0.4$ mg/mL, our samples exhibit the expected scaling law of $G' \sim C_c^{2.2}$ and lay within the range of published values (Fig. 2b).

To investigate the effect of adding microgels to collagen networks, we develop composite formulations where G' of the microgel component is less than or comparable to that of the collagen component; when packing pure microgels at concentrations above $C_m = 4.2$ % (w/w), we find the microgel elasticity dominates the contribution from collagen (Fig. 2c). Below $C_m = 4.2$ %, the microgels are dominantly fluid-like, exhibiting $G'' > G'$ (Fig. S2a). Adding collagen to the fluid-like microgels pushes the composite mixtures to the solid regime, where $G' > G''$. We also find that the composite materials exhibit frequency dependence in their complex modulus, $G^* = G' + i\,G''$, consistent with soft glassy rheology (SGR) at low frequencies and rigid polymer networks at high frequencies (Fig. S4). This type of frequency response resembles the rheology of living cells, which we explore further in the Discussion at the end of this manuscript. By contrast, the frequency dependent moduli of neither collagen nor packed microgels in isolation are well described by the SGR / polymer physics phenomenology (Fig. S4).

To test the scaling of G' in the composite material with increasing collagen concentration, C_c, and increasing microgel concentration, C_m, we choose a representative oscillation frequency of 0.1 Hz and plot G' versus C_m, creating a data series for each value of C_c. We observe clear separation between the different data series, finding that G' increases strongly with increasing C_c. To quantify the effect of adding microgels to collagen networks, we freely fit a power law to each dataset corresponding to a given value of C_c, finding that G' scales with C_m to an average power of 2.4 ± 0.2 (mean $\pm$ standard deviation across five datasets). With this analysis, we rescale the G' datasets by $C_m^{2.4}$, which collapse to a single power law of $G' \sim C_c^{2.9}$ (Fig. 2d). This empirical process reveals a scaling for the composite's storage modulus given by $G' \sim C_m^{2.4} \times C_c^{2.9}$. This enhanced scaling of storage modulus with collagen concentration has not been observed previously and demonstrates the synergistic effects of collagen-microgel mixtures. We hypothesize that the synergistic effect arises from the fact that pure collagen networks are known to be sub-isostatic, where the number of degrees of freedom exceeds the number of constraints; adding microgels to the network may increase the number of constraints, leading to the stronger scaling of modulus with collagen concentration [37].

2.2 Non-linear rheology and shape memory

Among the remarkable properties of biopolymer networks is their strain stiffening behavior, while among of the most useful properties of packed microgels is their yielding behavior. Both these phenomena emerge with increasing levels of imposed strain. Thus, we perform a series of high-strain rheological tests designed to elucidate how the reconfigurability of microgels and the strain-stiffening of collagen gels contribute to the non-linear behaviors of the composite material. While we focus here on microgel concentrations slightly below the close-packing concentration, confocal microscopy images suggest that the space occupied by the collagen network and the connectivity it provides

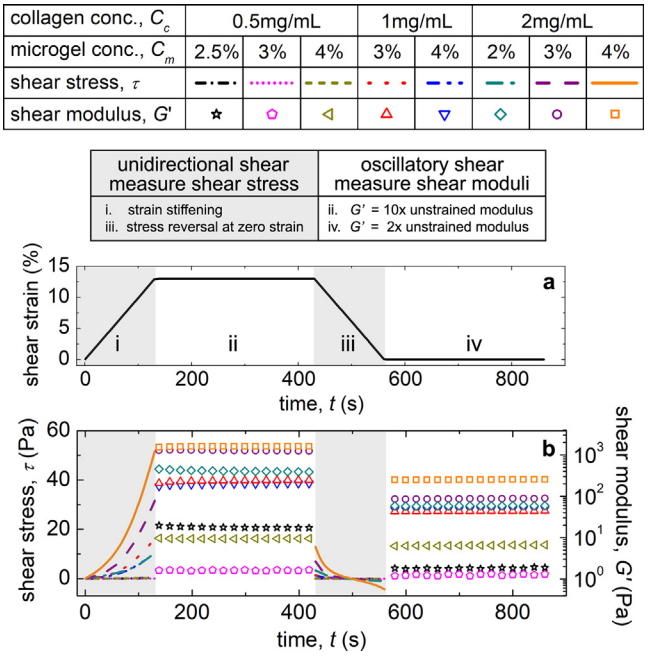

Fig. 3

High-strain rheology and stress reversal behavior of collagen-microgel composite materials. (a) Strain profile indicating (i) slow ramp of shear strain to 13 % followed by (ii) oscillations at 0.5 % strain amplitude and 1 Hz to measure *G'*, and (iii) slow ramp down of strain back to zero, followed by (iv) oscillations at 0.5 % strain amplitude and 1 Hz to measure *G'*. (b) The material stiffens as the applied strain ramps up to 13 %, and the elastic shear modulus remains steady through oscillations in the pre-strained state, indicating that the material shows a linear behavior. As the pre-strained material is sheared back to its original state, we observe an interesting behavior where stress reverses and goes negative at a finite strain. The elastic modulus is steady through oscillations but a factor of 2 higher than the modulus measured before any strain is applied, indicating small amounts of prestress stored in the material.

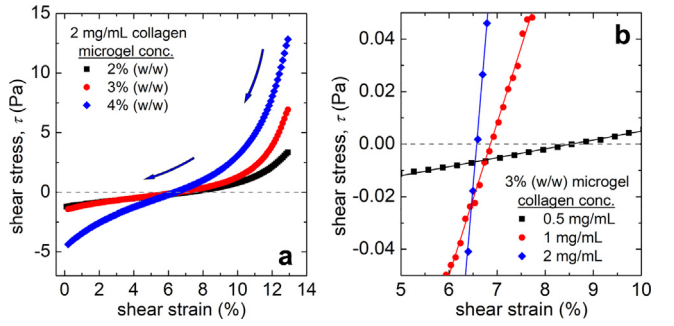

Fig. 4

Collagen-microgel composites exhibit stress reversal at a positive strain following the application of a large strain and reversal back to the original state. (a) Stress reversal for composites with 2 mg/mL collagen and varying microgel concentrations. The slope decreases with decreasing microgel concentrations due to decreasing elastic shear modulus. (b) Stress reversal for composites with 3 % (w/w) microgel and varying collagen concentrations. The zero-stress point occurs at higher strain values for composites having less collagen since softer networks require more strain than stiffer networks to achieve the same level of tension.

create an increased effective volume per microgel particle. Thus, we hypothesized that the collagen-microgel composite material would cross over into a different regime of material response at applied strain levels in which particles rearrange. We estimate this strain level to be approximately 13 %, as described in previous work [38]. Briefly, this strain corresponds to the scale of deformation required for close-packed, monodisperse spheres to slide past their nearest neighbors, divided by the sphere diameter; here this diameter would be an effective diameter. We slowly ramp shear strain up to 13 % over the course of 130 s, then superimpose small-amplitude oscillations at 0.5 % strain amplitude and 1 Hz, measuring *G'* of the pre-strained sample over time. After 300 s, the pre-strain is ramped back down to zero strain, where *G'* is measured again at 0.5 % strain amplitude and 1 Hz for 300 s (Fig. 3).

We find that as the applied strain ramps linearly in time to 13 %, the measured stress rises non-linearly, indicating that the composite samples are strain-stiffening (region *i* in Fig. 3). Once the sample is strained by 13 %, we find the elastic modulus has increased by approximately an order of magnitude and remains steady over the 300 s testing duration, oscillating at a frequency of 1 Hz and a super-imposed strain amplitude of 0.5 %, exhibiting no major relaxations (region *ii*, Fig. 3). As the rheometer geometry is rotated back to zero angular deflection, we observe an interesting material behavior where stress reverses sign, going negative at a finite-positive angle that corresponds to a shear strain in the range of 6 - 9 % (region *iii*, Fig. 3a; Fig. 4). Finally, after the rheometer geometry is returned to zero-angular deflection, which we call here the "zero-strain" state, we find that *G'* remains steady over time (region *iv*, Fig. 3), but remains 1.5 ± 0.24 times the original values measured before the strain-ramp test (mean ± standard deviation across 8 samples).

Most tested samples exhibit stress-reversal behavior following a large strain, crossing over to negative stresses within the range of 6 - 9 % positive strain during the ramp-down. We hypothesize that this zero-crossing and stress-reversal arises from the particles having re-arranged at high strain, resisting shear in the returning direction of the rheometer tool, while the tensed collagen network continues to pull back toward a zero-shear state, producing a meta-stable state of deformation in the composite material. Correspondingly, we find that the zero-stress point occurs at higher strain values for composites having less collagen; softer networks require more strain than stiffer networks to achieve the same level of balancing tension (Fig. 4). To test the robustness of the high-strain rheology and stress reversal behavior of the composites, we repeat the experiments at 25 °C and 30 °C and find no appreciable changes in the rheological behavior (Fig. S7).

To further test this idea of counteracting forces within the composite material after large strains, we perform strain ramp protocols like those in Fig. 3, but with one change: after the strain is ramped to 13 % and held for 300 s, the strain is ramped back down until the rheometer measures zero torque, which is recorded as zero-stress but a finite strain within the 6 - 9 % range (Fig. 5). Small-amplitude oscillations are then performed about this strain for 300 s, measuring *G'* at a frequency of 1 Hz and 0.5 % strain amplitude. Here, we find that *G'* exhibits no major relaxations and equals 0.85 ± 0.14 times the original values measured before the strain ramp (mean ± standard deviation over 3 different

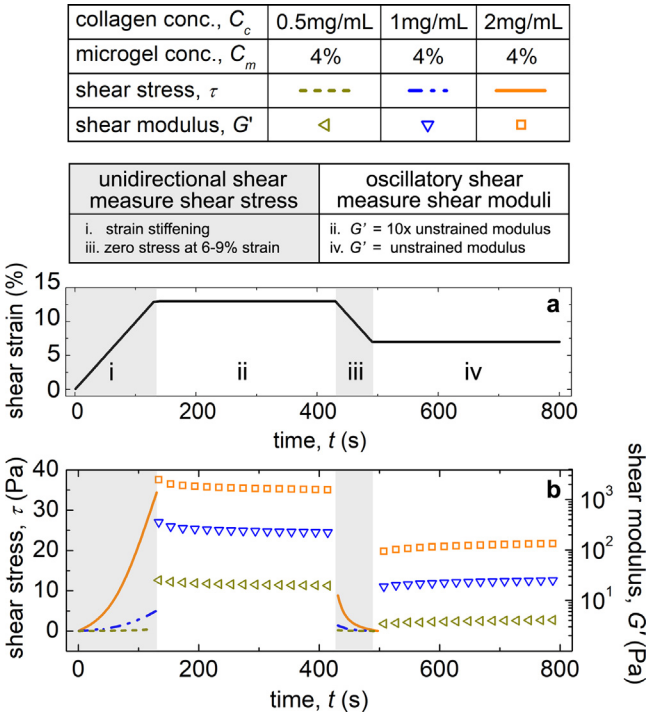

Fig. 5

High-strain rheology and zero stress at a finite strain for collagen-microgel composites. (a) Strain profile indicating (i) slow ramp of shear strain to 13 % followed by (ii) oscillations at 0.5 % strain amplitude and 1 Hz to measure G', and (iii) slow ramp down of strain back to a finite value where shear stress is zero, followed by (iv) oscillations at 0.5 % strain amplitude and 1 Hz to measure G'. (b) The material behavior in regions (v) and (vi) is similar to that in regions (i) and (ii), respectively; however, the elastic modulus at a finite strain where stress is zero is comparable to the modulus measured before strain is applied to the material. This indicates that the composite materials exhibit a shape memory behavior.

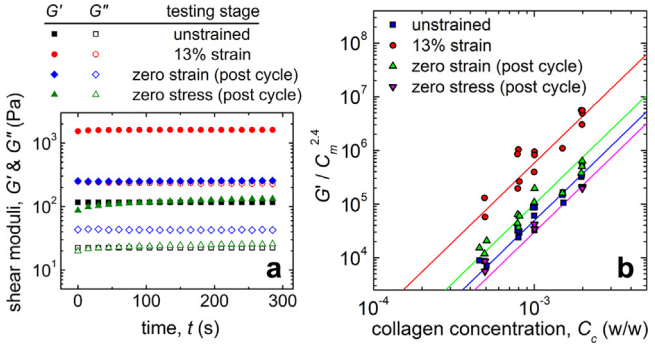

Fig. 6

Shear moduli of collagen-microgel composite materials with $C_c = 2$ mg/mL and $C_m = 4$ % (w/w), at different testing stages. (a) Shear moduli exhibit no major relaxations over 300 s at the different testing stages – before strain, 13 % strain, zero strain (post cycle), and zero stress (post cycle). (b) Elastic shear moduli rescaled with microgel concentration collapses into separate groups indicating a scaling of $G' \sim C_c^{2.9}$.

samples). Thus, in this state, a finite strain is "locked in" yet the sample exhibits no apparent stiffening; shearing the sample further toward the original zero strain state would soon result in measuring a negative shear stress and the sample exhibiting strain-stiffening, as seen above. Together, these observations indicate that in the ideal model scenario, the collagen network always has the same reference point for zero-stress, while the microgels' reference point resets following particle rearrangement events.

As a direct demonstration of how G' depends on these different levels of applied strain over time, we overlay small amplitude oscillatory shear data for a sample formulated at $C_c = 2$ mg/mL and $C_m = 4$ % (w/w), where C_c and C_m are the collagen and microgel concentrations as defined earlier. The shear moduli shown here exhibit little time-dependence relative to the separation between datasets and follow the same pattern as the averages described above (Fig 6a). To systematically investigate how the composite materials strain-stiffen and recover after large strains, we re-scale all the measurements of G' performed under different states of strain, dividing by $C_m^{2.4}$. We find the data collapse into separate groups, each of which exhibits scaling consistent with $G' \sim C_c^{2.9}$, as previously found. The samples pre-strained to 13 % exhibit the highest moduli laying on a curve 11.8 times the curve corresponding to unstrained samples; the samples at zero strain exhibit moduli twice the values measured before any strain is applied and the samples at zero stress have moduli 0.6 times the original values measured before the strain ramp test. Together, these results demonstrate that a wide range of collagen-microgel composite material compositions can be made to possess the most useful properties of their constituents, simultaneously; the composite material strain stiffens at intermediate strain levels, like typical biopolymer networks, while exhibiting reconfigurability, like typical jammed particulate materials. By combining the two, the material possesses mechanical programmability and shape memory; the material can be "locked into" states of stress that neither of the individual constituents are capable of maintaining alone.

2.3 Soft, submerged, shape-programmable structures

To assess how the rich rheological behaviors of this material provide may be used in applications, we fabricate simple structures and study how they perform after large strains. Composites consisting of 2 mg/mL collagen and 4 % (w/w) microgels are prepared as outlined in Section 2.2 and poured into 3D printed Acrylonitrile Butadiene Styrene (ABS) rectangular molds of dimensions 80 mm x 25 mm x 2 mm and 80 mm x 25 mm x 5 mm. After curing at 37^{0}C for two hours, the casted sheets are removed from the molds using a spatula and immersed in water. We find the casted materials are robust and can be manually reshaped at room temperature.

We conduct several tests to evaluate the material's shape retention capabilities. First, we bend a 5 mm thick rectangular sheet around a cylindrical stainless-steel rod and after 6 h we find that the material holds its bent shape (Fig. 7a). In a subsequent test, we bend a 2 mm thick rectangular sheet around a cylindrical rod but flip the sheet along the axis normal to the curvature and the material holds its shape for 24 h. We then flip the sheet 180°, and the material still holds shape for an additional 24 h (Fig. 7b). In another test, we make a loop out of a 2 mm thick sheet and rest it on its side; we find that the material holds its curved shape for 30 h. Finally, we make a bridge-shaped structure

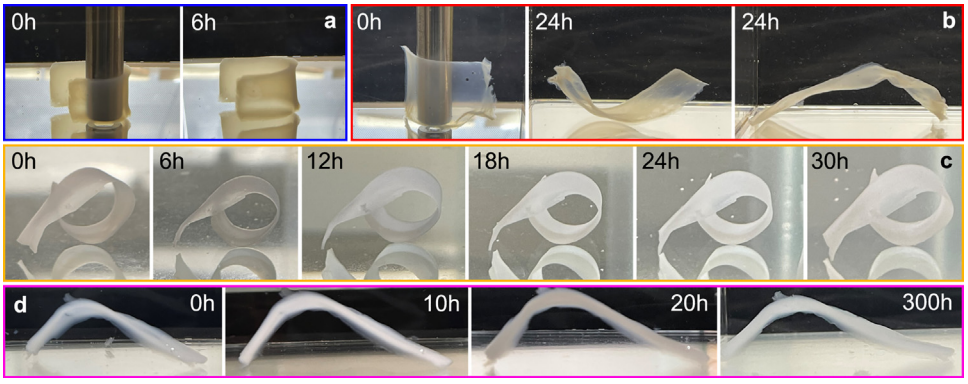

Fig. 7

Soft, shape-programmable structures casted out of composite materials consisting of 2 mg/mL collagen and 4 % (w/w) microgels, submerged in water. (a) A 5 mm thick rectangular sheet bent around a cylindrical stainless-steel rod holds its shape after 6 h. (b) A 2 mm thick rectangular sheet bent around a cylindrical rod and oriented concave-up holds its shape for 24 h. The same sheet flipped 180° still holds its shape for 24 h. (c) A loop made from 2 mm thick rectangular sheet and resting on its side holds its curved shape for 30 h. (d) A bent sheet holds its shape for 300 h.

and find that the material again holds its shape for 300 h. To assess if deformations of the composites lead to changes in birefringence as a functional property, we capture images of rectangular sheets casted out of the composite materials before and after applying strain while mounted between crossed-polarizers on a microscope. At zero-strain, we observed no detectable birefringence; at an extension strain of approximately 50 %, we observed very modest signs of birefringence. (Fig. S6). These experiments underscore the unique shape programmable attributes of the collagen-microgel composite materials, that can be leveraged to manufacture stable structures, impossible to make with collagen or microgels alone.

3 Discussion and conclusions

Here we have formulated a soft biocomposite material having physical properties derived from the non-linear behaviors of its two main constituents: a collagen-1 network and packed microgel particles. This material's elastic shear modulus depends strongly on its state of strain, which is typical of many biopolymer networks. By packing soft microgel particles into the biopolymer network, the non-linear states of strain stiffening can be self-maintained. Thus, the material exhibits a form programmability with respect to its shape and elasticity, simultaneously. Ideally, if the network component of the biocomposite maintains its detailed connectivity, it also has shape memory, which is reflected by the reversibility of the nonlinear effects we observe. There is a rich phenomenology of memory and programmability in materials [39], including demonstrations of materials that appear to learn in response to the details of mechanical shearing [40]. We envision that the material we have made here can be used as a model system to test emerging ideas about memory and learning in mechanical systems, as well as find use in applications. For example, simple sheets made from this material can be bent and manually shaped in analogy to metallic foils, exhibiting no signs of large-scale relaxation over time. This biocomposite material could inspire designs in biomedical applications such as cartilage and tissue regeneration or vascular structure formation, where form-fitting scaffolds are beneficial [41–43] and where maintaining a low matrix concentration would assist in mitigating fibrosis or inflammatory responses [44–47]. Finally, to create complex structures that are more robust and mechanically defined than structures made from their individual constituents, this material could be 3D bioprinted; previous work has demonstrated the ability of printing low concentration collagen [48], pure microgel packs [49], and mixtures of cells and collagen [5,50], indicating that the biocomposites described here could be printed using the same simple approaches while achieving the same structural precision.

Expecting to draw parallels with the rheological responses of biological tissue, as observed previously, we were surprised to find connections to the rheology of individual living cells; both systems strain-stiffen and the frequency-dependent complex moduli of our biocomposite materials obey scaling laws very close to those found in rheological measurements performed on individual cells [19,51]. The complex modulus of both materials exhibit weak power-law scaling at low frequencies, as described by rheological models of soft glasses, and stronger power-law dependence at high frequencies, associated with the constituent polymer networks. In some respects, this similarity may be expected: like our biocomposite material, the cytoskeletal network is permeated with a complex fluid, the cytoplasm. Indeed, a large body of work has shown that the crowded proteins dispersed throughout cytoplasm exhibit signs of glassy dynamics [17,19,51–53]. There are many key differences to take note of, however. The collagen-1 networks we use are not constantly remodeling like the cytoskeleton; the rheological crossover between SGR and polymer network elasticity in the cell is attributed to the time-scale associated with such remodeling. Likewise, the cytoskeletal F-actin filaments are semi-flexible polymers, whereas the collagen-1 fibers fall closer to the classification of rigid polymers and have been treated as athermal elastic rods [37]. Finally, the proteins of the cytoplasm, even if crowded to the point of exhibiting glassy behaviors, are nano-scale and thus thermally active. The microgels we use are much larger than 1 μm and can be thought of as athermal soft granules. Keeping these differences in mind, we are intrigued by the possibility that the collagen/microgel composite

material we investigated here could be considered a minimal, athermal, rheological model of the cell. Such a model could be useful to further elucidate certain striking cell behaviors, such as the "unjamming" of cells in compressed monolayers following the removal of pressure from the apical surface [18,54]. If compressing the cytoskeleton-cytoplasm composite within living cells leads to the arrest of cell motion through a mechanism analogous the shape-programmability found in our material, the same mechanism could be used to design a diversity of highly tunable and reconfigurable materials inspired by the cell.

4 Materials and methods

4.1 Microgel synthesis

To synthesize PEG microgels, a solution of 25 % (w/w) poly(ethylene glycol) methyl ether acrylate (Mn = 480 g mol-1, Sigma Aldrich 454,990), 0.4 % (w/w) poly(ethylene glycol) diacrylate (Mn = 700 g mol-1, Sigma Aldrich 455,008), and 0.15 % (w/w) ammonium persulfate (Sigma Aldrich A3678) is prepared in ultrapure water. Separately, a 0.7 % (w/w) polyglycerol polyricinoleate (a commercial surfactant, Paalsgaard PGPR-4125) solution is prepared in kerosene. The aqueous and organic solutions are then combined in a beaker, placed on an ice bath, and homogenized at 8000 rpm for 5 min to form a milky-white emulsion. Nitrogen is bubbled through the covered solution for 1 hour to displace dissolved oxygen. The deoxygenated reaction mixture is removed from ice and transferred to a 1 L round bottom flask equipped with a magnetic stirring bar. At this time, 0.5 % (w/w) of 1,2-Di(dimethylamino)ethane (TEMED, Fisher Scientific BP150) is added dropwise while the solution is stirred in a nitrogen atmosphere for 1 hour. The solution is then exposed to air and stirred for 30 min to complete the reaction. To separate the microgels from the kerosene phase, methanol is added to the microgel solution, and the mixture is vigorously shaken in 500 mL centrifuge tubes followed by centrifugation at 4000 x g for 15 min and removal of supernatant; these washing steps are performed three times to completely remove the surfactant and organic phases. Finally, PBS is used in the same washing, centrifugation, and supernatant removal steps two times. The microgel solution is then sterilized by autoclaving for 30 min in a liquid cycle at 120 °C and 15 psi. The autoclaved microgels are left at room temperature in a biosafety cabinet until temperature equilibration and aliquoted in 50 mL centrifuge tubes.

4.2 Microgel / collagen composite formulation

The PEG microgels are lyophilized and reconstituted at 12 % (w/w) in sterile PBS. The microgel solution is mixed with 25 μM HEPES buffer, PBS, and cold collagen (Nutragen Type I Collagen Solution 6 mg/mL, Advanced Biomatrix 5010) such that the final concentrations of collagen and microgels are the desired concentrations for the composite formulation. The fraction of each component is precisely measured by weighing them on a microbalance. Small volumes of NaOH (less than 1 % of the total mixture volume) are added to neutralize the pH, and the material is mixed in a planetary speed mixer at 3500 rpm for 2 min. The composite material is then transferred to ice until experiments are performed.

4.3 Rheology

Material properties of the collagen-microgel composites are measured by conducting shear rheology experiments on an Anton Paar MCR 702 rheometer. The composite material is gelled on the rheometer at 37^0C prior to the experiment. Sample evaporation is prevented by a solvent trap and the sample is maintained at 37^0 C throughout the experiment using a Peltier temperature control system. A 50 mm sandblasted cone-plate geometry with a measuring gap of 98 μm is used for collagen concentrations below 1 mg/mL and a 50 mm sandblasted parallel-plate geometry with a measuring gap of 1 mm is used for other material compositions. Shear moduli of the composite materials are measured under oscillatory shear at 2 % strain amplitude and 0.1–10 Hz frequency. Nonlinear stress-strain relationships are probed using unidirectional strain ramps. Rheological tests on samples in pre-stressed states are performed by ramping the shear strain from 0 % to 13 %, followed by a super-imposed oscillatory test of the strained material at 0.5 % strain amplitude and 1 Hz. To test for reversibility, these pre-strain samples are returned to zero strain or zero stress, followed by an oscillatory test of the relaxed material at 0.5 % strain amplitude and 1 Hz frequency.

4.4 Microscopy and photography

To image the composite material structure, 3D stacks of fluorescence and reflectance images are collected using a Nikon Eclipse Ti-2 laser scanning confocal microscope with a C2+ scan head and a 60x oil objective with a numerical aperture (NA) of 1.4. We collect images with a spatial sampling resolution of 0.2 μm per pixel in the X–Y plane and 0.25 μm per step in the Z direction. Microgels conjugated with rhodamine B acrylate (Polysciences 25,404–100) are imaged using a TRITC fluorescence filter configuration; collagen fibers are imaged using a confocal reflectance filter configuration. To remove random noise, the individual channel images are blurred with a Gaussian kernel having a half-width of 0.7 pixels. We then take the logarithm of the maximum intensity projection of approximately 50 slices along the z-axis and overlay the channels to generate the composite image. Photographs of the casted composite sheets are taken using a Canon digital camera.

Declaration of competing interest

The authors declare that they have no known competing financial interests or personal relationships that could have appeared to influence the work reported in this paper.

Data Availability

Data will be made available on request.

CRediT authorship contribution statement

Vignesh Subramaniam: Writing – original draft, Validation, Software, Methodology, Investigation, Formal analysis. **Abhishek M. Shetty:** Validation, Methodology, Formal analysis. **Steven J. Chisolm:** Investigation, Formal analysis. **Taylor R. Lansberry:** Investigation, Formal analysis. **Anjana Balachandar:** Formal analysis. **Cameron D. Morley:** Methodology. **Thomas E. Angelini:** Writing – original draft,

Supervision, Project administration, Methodology, Funding acquisition, Formal analysis, Conceptualization.

Acknowledgements

The authors thank Anton Paar for the use of the Anton Paar 702 rheometer through their VIP academic research program. This research was supported by the National Science Foundation via the REU Site: Engineering for Healthcare EEC-1757128. Research was sponsored by the Office of the Secretary of Defense and was accomplished under Agreement Number W911NF-17–3–0003. The views and conclusions contained in this document are those of the authors and should not be interpreted as representing the official policies, either expressed or implied, of the Office of the Secretary of Defense or the U.S. Government. The U.S. Government is authorized to reproduce and distribute reprints for Government purposes notwithstanding any copyright notation herein.

Supplementary materials

Supplementary material associated with this article can be found, in the online version, at doi:10.1016/j.giant.2024.100297.

References

[1] Y-l Yang, L.M. Leone, L.J. Kaufman, Elastic moduli of collagen gels can be predicted from two-dimensional confocal microscopy, Biophys. J. 97 (7) (2009) 2051–2060.

[2] Y-l Yang, L.J. Kaufman, Rheology and confocal reflectance microscopy as probes of mechanical properties and structure during collagen and collagen/hyaluronan self-assembly, Biophys. J. 96 (4) (2009) 1566–1585.

[3] A.M. Stein, D.A. Vader, D.A. Weitz, L.M. Sander, The micromechanics of three-dimensional collagen-I gels, Complex. 16 (4) (2011) 22–28.

[4] S. Motte, L.J. Kaufman, Strain stiffening in collagen I networks, Biopolymers 99 (1) (2013) 35–46.

[5] C.D. Morley, S.T. Ellison, T. Bhattacharjee, C.S. O'Bryan, Y. Zhang, K.F. Smith, et al., Quantitative characterization of 3D bioprinted structural elements under cell generated forces, Nat. Commun. 10 (1) (2019) 3029.

[6] A.J. Licup, S. Münster, A. Sharma, M. Sheinman, L.M. Jawerth, B. Fabry, et al., Stress controls the mechanics of collagen networks, Proc. Natl. Acad. Sci. 112 (31) (2015) 9573–9578.

[7] A.S. Van Oosten, M. Vahabi, A.J. Licup, A. Sharma, P.A. Galie, F.C. MacKintosh, et al., Uncoupling shear and uniaxial elastic moduli of semiflexible biopolymer networks: compression-softening and stretch-stiffening, Sci. Rep. 6 (1) (2016) 1–9.

[8] T. Golde, C. Huster, M. Glaser, T. Händler, H. Herrmann, J.A. Käs, et al., Glassy dynamics in composite biopolymer networks, Soft Matter 14 (39) (2018) 7970–7978.

[9] Y.-C. Lin, G.H. Koenderink, F.C. MacKintosh, D.A. Weitz, Control of non-linear elasticity in F-actin networks with microtubules, Soft Matter 7 (3) (2011) 902–906.

[10] C. Storm, J.J. Pastore, F.C. MacKintosh, T.C. Lubensky, P.A. Janmey, Nonlinear elasticity in biological gels, Nature 435 (7039) (2005) 191–194.

[11] Treloar L.G. The physics of rubber elasticity. 1975.

[12] Y-l Wang, D.E. Discher, Cell Mechanics, Academic press, 2007.

[13] J. Stricker, T. Falzone, M.L. Gardel, Mechanics of the F-actin cytoskeleton, J. Biomech. 43 (1) (2010) 9–14.

[14] M.L. Gardel, F. Nakamura, J. Hartwig, J.C. Crocker, T.P. Stossel, D.A. Weitz, Stress-Dependent elasticity of composite actin networks as a model for cell behavior, Phys. Rev. Lett. 96 (8) (2006) 088102.

[15] O. Chaudhuri, S.H. Parekh, D.A. Fletcher, Reversible stress softening of actin networks, Nature 445 (7125) (2007) 295–298.

[16] P.A. Janmey, M.E. McCormick, S. Rammensee, J.L. Leight, P.C. Georges, MacKintosh FC. Negative normal stress in semiflexible biopolymer gels, Nat. Mater. 6 (1) (2007) 48–51.

[17] B. Fabry, G.N. Maksym, J.P. Butler, M. Glogauer, D. Navajas, J.J. Fredberg, Scaling the microrheology of living cells, Phys. Rev. Lett. 87 (14) (2001) 148102.

[18] P. Bursac, G. Lenormand, B. Fabry, M. Oliver, D.A. Weitz, V. Viasnoff, et al., Cytoskeletal remodelling and slow dynamics in the living cell, Nat. Mater. 4 (7) (2005) 557–561.

[19] L. Deng, X. Trepat, J.P. Butler, E. Millet, K.G. Morgan, D.A. Weitz, et al., Fast and slow dynamics of the cytoskeleton, Nat. Mater. 5 (8) (2006) 636–640.

[20] M.L. Gardel, F. Nakamura, J.H. Hartwig, J.C. Crocker, T.P. Stossel, D.A. Weitz, Prestressed F-actin networks cross-linked by hinged filamins replicate mechanical properties of cells, Proc. Natl. Acad. Sci. 103 (6) (2006) 1762–1767.

[21] G.H. Koenderink, Z. Dogic, F. Nakamura, P.M. Bendix, F.C. MacKintosh, J.H. Hartwig, et al., An active biopolymer network controlled by molecular motors, Proc. Natl. Acad. Sci. 106 (36) (2009) 15192–15197.

[22] D. Humphrey, C. Duggan, D. Saha, D. Smith, J. Käs, Active fluidization of polymer networks through molecular motors, Nature 416 (6879) (2002) 413–416.

[23] D. Mizuno, C. Tardin, C.F. Schmidt, MacKintosh FC. Nonequilibrium mechanics of active cytoskeletal networks, Science 315 (5810) (2007) 370–373.

[24] A.R. Bausch, K. Kroy, A bottom-up approach to cell mechanics, Nat. Phys. 2 (4) (2006) 231–238.

[25] N. Wang, I.M. Tolic-Nørrelykke, J. Chen, S.M. Mijailovich, J.P. Butler, J.J. Fredberg, et al., Cell prestress. I. Stiffness and prestress are closely associated in adherent contractile cells, Am. J. Physiol.-Cell Physiol. 282 (3) (2002) C606-C16.

[26] K.E. Kasza, A.C. Rowat, J. Liu, T.E. Angelini, C.P. Brangwynne, G.H. Koenderink, et al., The cell as a material, Curr. Opin. Cell Biol. 19 (1) (2007) 101–107.

[27] H. Jia, J. Flommersfeld, M. Heymann, S.K. Vogel, H.G. Franquelim, D.B. Brückner, et al., 3D printed protein-based robotic structures actuated by molecular motor assemblies, Nat. Mater. 21 (6) (2022) 703–709.

[28] G. Henkin, S.J. DeCamp, D.T. Chen, T. Sanchez, Z. Dogic, Tunable dynamics of microtubule-based active isotropic gels, Philos Trans A Math Phys Eng Sci 372 (2029) (2014).

[29] C. Darkes-Burkey, X. Liu, L. Slyker, J. Mulderrig, W. Pan, E.P. Giannelis, et al., Simple synthesis of soft, tough, and cytocompatible biohybrid composites, Proc. Natl. Acad. Sci. 119 (28) (2022) e2116675119.

[30] T. Hu, A.C.Y. Lo, Collagen–alginate composite hydrogel: application in tissue engineering and biomedical sciences, Polymers (Basel) 13 (11) (2021) 1852.

[31] B. Carroll, M.-T.H. Thanh, A.E. Patteson, Dynamic remodeling of fiber networks with stiff inclusions under compressive loading, Acta Biomater. (2022).

[32] J.L. Shivers, J. Feng, A.S.G. van Oosten, H. Levine, P.A. Janmey, MacKintosh FC. Compression stiffening of fibrous networks with stiff inclusions, Proc. Natl. Acad. Sci. 117 (35) (2020) 21037–21044.

[33] N.A.K. Bharadwaj, J.G. Kang, M.C. Hatzell, K.S. Schweizer, P.V. Braun, R.H. Ewoldt, Integration of colloids into a semi-flexible network of fibrin, Soft Matter 13 (7) (2017) 1430–1443.

[34] M.R. Islam, R.C. Picu, Random fiber networks with inclusions: the mechanism of reinforcement, Phys. Rev. E 99 (6) (2019) 063001.

[35] G. Chaudhary, A. Ghosh, N.A. Bharadwaj, J.G. Kang, P.V. Braun, K.S. Schweizer, et al., Thermoresponsive stiffening with microgel particles in a semiflexible fibrin network, Macromolecules 52 (8) (2019) 3029–3041.

[36] R.C. Arevalo, J.S. Urbach, D.L. Blair, Size-dependent rheology of type-I collagen networks, Biophys. J. 99 (8) (2010) L65–L67.

[37] J.L. Shivers, S. Arzash, A. Sharma, F.C. MacKintosh, Scaling theory for mechanical critical behavior in fiber networks, Phys. Rev. Lett. 122 (18) (2019) 188003.

[38] T. Bhattacharjee, C.P. Kabb, C.S. O'Bryan, J.M. Urueña, B.S. Sumerlin, W.G. Sawyer, et al., Polyelectrolyte scaling laws for microgel yielding near jamming, Soft Matter 14 (9) (2018) 1559–1570.

[39] N.C. Keim, J.D. Paulsen, Z. Zeravcic, S. Sastry, S.R. Nagel, Memory formation in matter, Rev. Mod. Phys. 91 (3) (2019) 035002.

[40] N.C. Keim, J.D. Paulsen, Multiperiodic orbits from interacting soft spots in cyclically sheared amorphous solids, Sci. Adv. 7 (33) (2021) eabg7685.

[41] P. Hu, A. Chiarini, J. Wu, Z. Wei, U. Armato, Dal Prà I. adult human vascular smooth muscle cells on 3D silk fibroin nonwovens release exosomes enriched in angiogenic and growth-promoting factors, Polymers (Basel) 14 (4) (2022) 697.

[42] A. Serafim, S.I. Voicu, Scaffolds and surfaces with biomedical applications, Polymers (Basel) 15 (9) (2023) 2126.

[43] M.V. Varma, B. Kandasubramanian, S.M. Ibrahim, 3D printed scaffolds for biomedical applications, Mater. Chem. Phys. 255 (2020) 123642.

[44] E.E. Beketov, E.V. Isaeva, N.D. Yakovleva, G.A. Demyashkin, N.V. Arguchinskaya, A.A. Kisel, et al., Bioprinting of cartilage with bioink based on high-concentration collagen and chondrocytes, Int. J. Mol. Sci. 22 (21) (2021) 11351.

[45] E.V. Isaeva, E.E. Beketov, G.A. Demyashkin, N.D. Yakovleva, N.V. Arguchinskaya, A.A. Kisel, et al., Cartilage formation in vivo using high concentration collagen-based bioink with msc and decellularized ECM granules, Int. J. Mol. Sci. 23 (5) (2022) 2703.

[46] E.V. Isaeva, E.E. Beketov, V.V. Yuzhakov, N.V. Arguchinskaya, A.A. Kisel, E.P. Malakhov, et al., The use of collagen with high concentration in cartilage tissue engineering by means of 3D-bioprinting, Cell tissue biol 15 (5) (2021) 493–502.

[47] J. Herrera, C.A. Henke, P.B. Bitterman, Extracellular matrix as a driver of progressive fibrosis, J. Clin. Invest. 128 (1) (2018) 45–53.

[48] Y. Zhang, S.T. Ellison, S. Duraivel, C.D. Morley, C.R. Taylor, T.E. Angelini, 3D printed collagen structures at low concentrations supported by jammed microgels, Bioprinting 21 (2021) e00121.

[49] C.S. O'Bryan, A. Brady-Miné, C.J. Tessmann, A.M. Spotz, T.E. Angelini, Capillary forces drive buckling, plastic deformation, and break-up of 3D printed beams, Soft Matter 17 (14) (2021) 3886–3894.

[50] C.D. Morley, C.T. Flores, J.A. Drake, G.L. Moore, D.A. Mitchell, T.E. Angelini, Spatiotemporal T cell dynamics in a 3D bioprinted immunotherapy model, Bioprinting 28 (2022) e00231.

[51] K. Nishizawa, M. Bremerich, H. Ayade, C.F. Schmidt, T. Ariga, D. Mizuno, Feedback-tracking microrheology in living cells, Sci. Adv. 3 (9) (2017) e1700318.

[52] K. Nishizawa, K. Fujiwara, M. Ikenaga, N. Nakajo, M. Yanagisawa, D. Mizuno, Universal glass-forming behavior of in vitro and living cytoplasm, Sci. Rep. 7 (1) (2017) 15143.

[53] B.R. Parry, I.V. Surovtsev, M.T. Cabeen, C.S. O'Hern, E.R. Dufresne, C. Jacobs-Wagner, The bacterial cytoplasm has glass-like properties and is fluidized by metabolic activity, Cell 156 (1–2) (2014) 183–194.

[54] B. Fabry, G.N. Maksym, J.P. Butler, M. Glogauer, D. Navajas, N.A. Taback, et al., Time scale and other invariants of integrative mechanical behavior in living cells, Phys. Rev. E 68 (4) (2003) 041914.

Supplementary Information

Biopolymer Networks Packed with Microgels Combine Strain Stiffening and Shape Programmability

Vignesh Subramaniam [a], Abhishek M. Shetty [b], Steven J. Chisolm [a], Taylor R. Lansberry [c], Anjana Balachandar [d], Cameron D. Morley [e], and Thomas E. Angelini [a, c, f, *]

a University of Florida, Herbert Wertheim College of Engineering, Department of Mechanical and Aerospace Engineering, Gainesville, FL, 32611, USA

b Advanced Technical Center, Anton Paar USA, Ashland, VA, 23005, USA

c University of Florida, Herbert Wertheim College of Engineering, J. Crayton Pruitt Family Department of Biomedical Engineering, Gainesville, FL, 32611, USA

d Stanford University, Department of Bioengineering, Stanford, CA, 94305, USA

e University of California Berkeley, Department of Bioengineering, Berkeley, CA, 94720, USA

f University of Florida, Herbert Wertheim College of Engineering, Department of Materials Science and Engineering, Gainesville, FL, 32611, USA

Email: t.e.angelini@ufl.edu

S1. Microgel Particle Size

The PEG microgels are synthesized as described in section 4.1, diluted in PBS buffer, and imaged with brightfield microscopy to measure the particle size and shape (Fig. S1a). We characterize the particle size distribution of these microgels through quantitative analysis of the brightfield images. Custom MATLAB segmentation code is used to detect particle edges and label each region of the image corresponding to a particle. The cross-sectional areas of all isolated objects are measured and tabulated; we equate each measured area to that of a circle and solve for the corresponding effective diameter, D. We then construct a probability density function of particle diameter, $p(D)$. We find that $p(D)$ follows a log-normal distribution, as previously found with similar materials [1]. The mode of the distribution lays at roughly 5 μm, while the mean diameter (± standard deviation) of the microgel particles is 9.46 ± 4.25 μm (Fig. S1b). This broad distribution may be important to the material's performance; if the microgel particles were monodisperse, the material may form crystalline domains having preferred directions of particle rearrangements. Such ordered domains would likely make the reconfigurability of the collagen-microgel composites anisotropic, resulting in materials with limited performance. By contrast, the broad particle size distribution of PEG microgels promotes isotropic particle rearrangements that enable the material properties we observe in the composite materials.

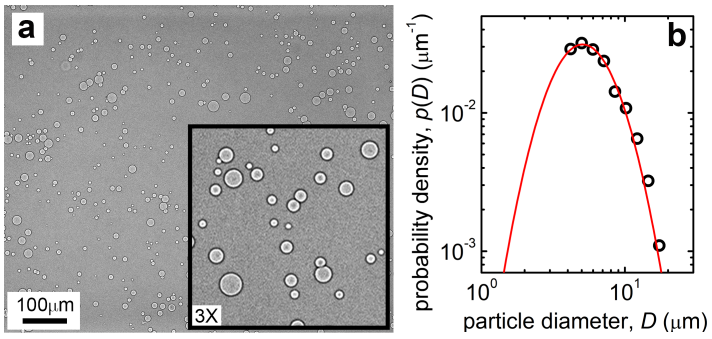

Figure S1. PEG microgels synthesized by inverse emulsion polymerization. (a) Brightfield image of microgels suspended in PBS. (b) The probability density function of particle diameter exhibits a mode at approximately 5 μm.

S2. Microgel Rheology

Rheological tests are performed on microgel dispersions prepared at a variety of concentrations using an Anton Paar MCR 702 rheometer with 25mm and 50mm parallel plate geometry. We perform small amplitude frequency sweeps to determine the elastic and viscous shear moduli in

the linear deformation regime. A strain amplitude of 1% is applied to the samples oscillating over a frequency range of 0.1-10Hz. Elastic shear moduli are larger than viscous moduli over a range of microgel concentrations above 4.2% (*w*/*w*), indicating that this is a crossover concentration where microgels transition from liquid-like to solid-like state (Fig. S2a); below this concentration the measured torque values fall below the instrument's sensitivity. To investigate the yielding of microgel packs under persistent shear, we perform unidirectional shear tests, ramping the shear rate from 0.001 to 100 s^{-1} while measuring the shear stress. We find the shear stress curves exhibit plateaus at low shear rates corresponding to the materials' yield stresses, falling within the approximate range of 0.1-10 Pa (Fig. S2b).

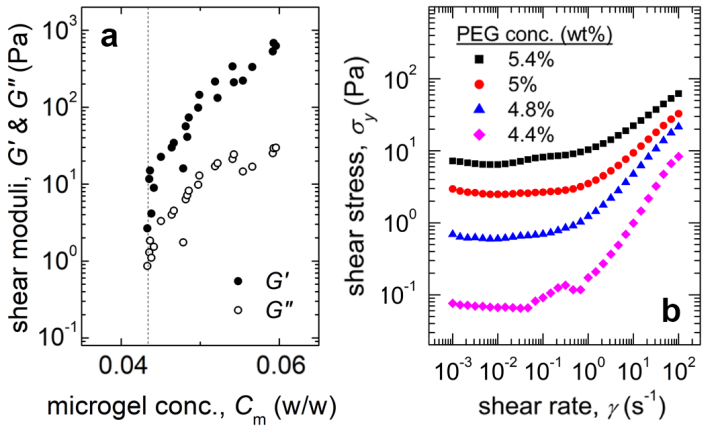

Figure S2. Material characterization of PEG microgels using shear rheology. (a) Elastic shear moduli of microgel solutions (G') are greater than viscous moduli (G") for a wide range of microgel concentrations, indicating that the material behaves like a damped elastic solid under low levels of shear. (d) The material exhibits low yield stress in the range of 0.1-10 Pa at concentrations above loose packing, and the yield stress of the material is linearly proportional to the elastic shear modulus.

S3. Collagen Rheology

Shear rheology experiments are performed on collagen networks prepared at different concentrations by mixing solutions of cold collagen (Nutragen Type I Collagen Solution 6mg/mL, Advanced Biomatrix 5010) with 25μM HEPES buffer, and PBS. The fraction of each component is precisely measured by weighing them on a microbalance. Small volumes of NaOH (less than 1% of the total mixture volume) are added to neutralize the pH, and the material is transferred to ice until experiments are performed. Collagen solutions are gelled on the rheometer at 37°C for 45 minutes prior to shear rheology tests. We measure shear moduli of the collagen gels using oscillatory frequency sweeps at a 2% strain amplitude and extract storage modulus, *G*', and loss modulus, *G*", spanning a frequency range of 0.1 Hz to 10 Hz. We find that

G' > G" and both G' and G" increase weakly with increasing frequency over most of this range (Fig. S3).

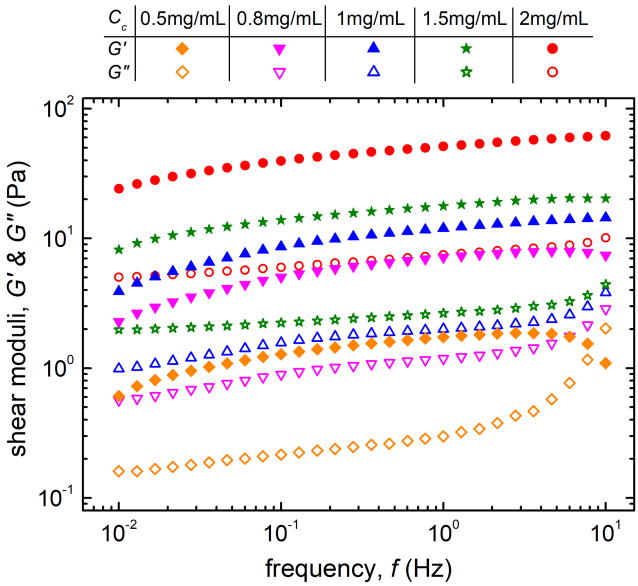

Figure S3. Material characterization of collagen gels using shear rheology. Oscillatory frequency sweeps are performed at a 2% strain amplitude spanning a frequency range of 0.1 Hz to 10 Hz. We find that G' > G" and both G' and G" increase weakly with increasing frequency over most of the frequency range.

S4. Soft Glassy Dynamics of Collagen-Microgel Composites and their Constituents

Drawing from prior work on the frequency-dependent moduli of the cytoskeleton / cytosol composite within living cells [2-4], we investigate the frequency dependence of collagen-microgel composites' moduli. For comparison, we also study the frequency dependent moduli of pure collagen and microgels, separately. We denote the complex modulus at frequency, f, by $G^*(f)$. A two-term power law model, given by $G^*(f) = A(if)^\alpha + B(if)^\beta$, is split into real and imaginary parts that are simultaneously fit to G' and G'' of each sample, with respect to parameters A, B, α, and β, while statistically weighting the imaginary part of the function. We find that the model does not fit the shear moduli of pure microgel samples at all. This can be understood from direct inspection; G' is nearly frequency-independent, which would force G'' toward zero in the fit, missing the corresponding data points (Fig. S4a). Similarly, the moduli of pure collagen networks exhibit weak non-monotonic frequency dependencies that the fits appear unable to satisfy simultaneously (Fig. S4b). However, the collagen-microgel composites exhibit G' curves that follow a weak frequency-dependent power law and G'' curves that follow two weak power-law regimes; the model is able to simultaneously capture both these shapes for each dataset.

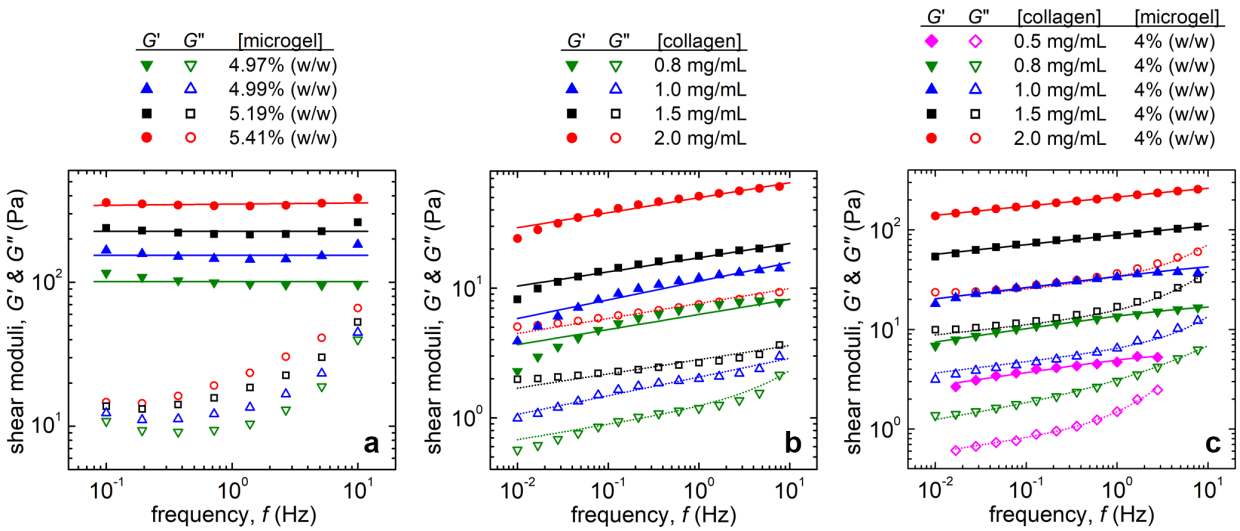

Figure S4. Soft glassy dynamics of collagen-microgel composites, pure collagen, and microgels. A two-term power law model, $G^*(f) = A(if)^{\alpha} + B(if)^{\beta}$ is fit to shear moduli of (a) microgels, (b) pure collagen solutions, and (c) collagen-microgel composites. Pure collagen solutions have weak frequency-dependent G' that manifests in the composites. G'' of composites follow two weak power-law regimes.

We find the average values of the α and β to be 0.105 and 1.05. Prior work on living cells found α to be within the range of 0.15 and 0.35, corresponding to soft glassy rheology at low frequencies, and β to be 0.75, corresponding to semiflexible polymer rheology at high frequencies [2, 4, 5]. Here, the composite materials exhibit β close to 1 at high frequencies, as found in the rheology of rigid networks [6-8], and a soft glassy behavior at low frequencies (Fig. S4c). The powers show no systematic trend with the overall stiffness of the samples, as seen in plots of α and β versus $|G^*|$, where a representative frequency of 0.1 Hz is chosen (Fig. S5). Thus, the general class of frequency-dependent rheology appears to emerge synergistically from the combination of materials and not from a particular composition or material concentration; the connection to soft glassy rheology suggests that the composite material possesses a complex landscape of local energy minima that neither of the two individual components possess on their own. We are intrigued by the rheological similarities between the collagen-microgel composite and the living cell, both exhibiting soft glassy rheological behavior at low frequencies and rheological responses of their constituent biopolymer networks at high frequencies.

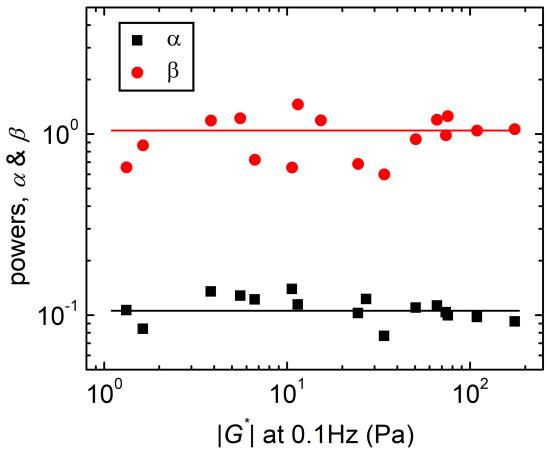

Figure S5. Powers α and β of the two-term model $G^*(f) = A(if)^{\alpha} + B(if)^{\beta}$ show no systematic trend with the absolute values of G^*.

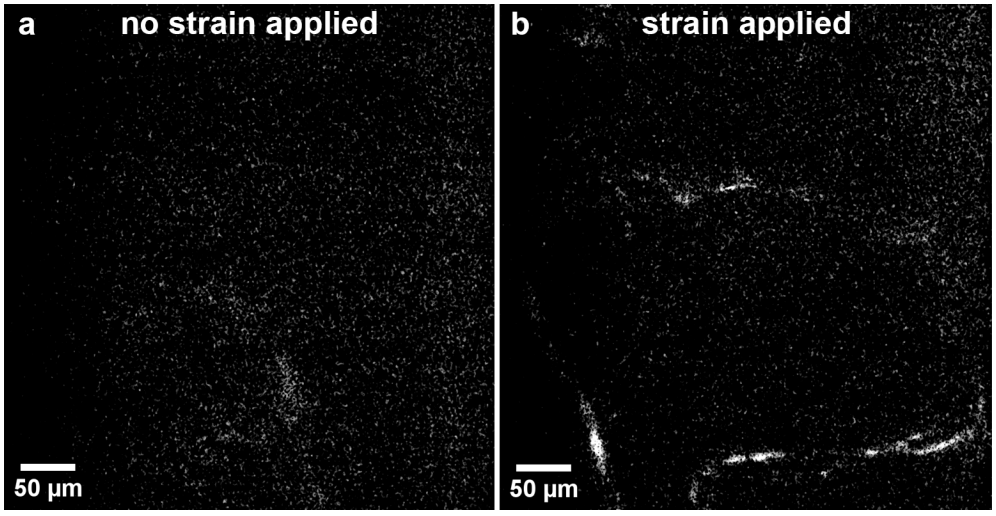

Figure S6. Images of a collagen-microgel composite sample mounted between crossed-polarizers on a microscope. (a) Unstrained sample shows no changes in birefringence, and (b) strained sample shows modest levels of changes in birefringence.

collagen conc., C_c	2mg/mL	2mg/mL	2mg/mL
microgel conc., C_m	4%	4%	4%
temperature, T	25°C	30°C	37°C
shear stress, τ			
shear modulus, G'			

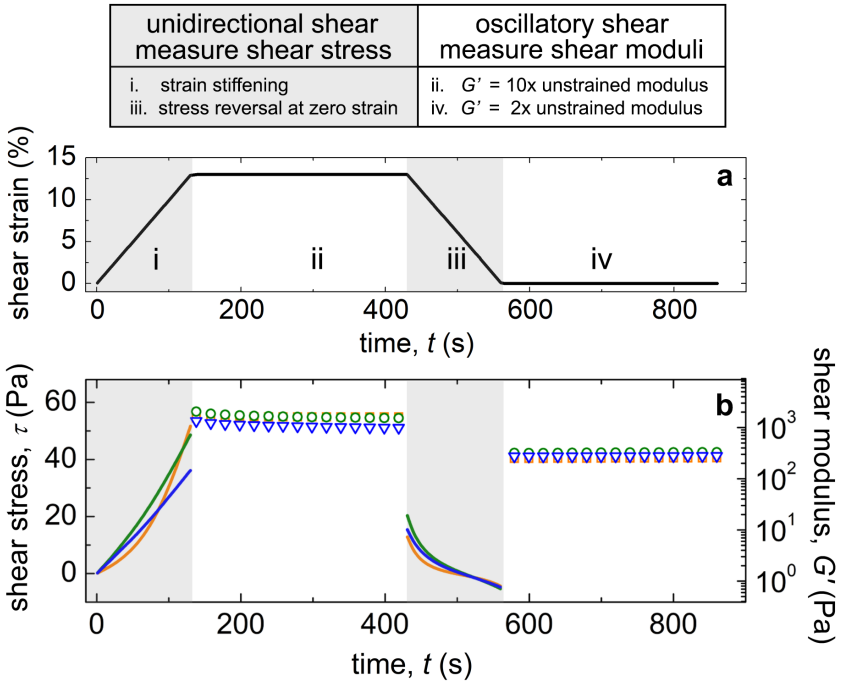

Figure S7. Temperature effects on high-strain rheology and stress reversal behavior of collagen-microgel composite materials. (a) Strain profile indicating (i) slow ramp of shear strain to 13% followed by (ii) oscillations at 0.5% strain amplitude and 1Hz to measure G', and (iii) slow ramp down of strain back to zero, followed by (iv) oscillations at 0.5% strain amplitude and 1 Hz to measure G'. (b) No appreciable changes are observed in the rheological behavior of the composites: the material stiffens as the applied strain ramps up to 13%, the elastic shear modulus remains steady through oscillations in the pre-strained state, and as the pre-strained material is sheared back to its original state, we observe stress reversal at a finite strain.

References

[1] Bhattacharjee T, Kabb CP, O'Bryan CS, Urueña JM, Sumerlin BS, Sawyer WG, et al. Polyelectrolyte scaling laws for microgel yielding near jamming. Soft Matter. 2018;14(9):1559-70.

[2] Deng L, Trepat X, Butler JP, Millet E, Morgan KG, Weitz DA, et al. Fast and slow dynamics of the cytoskeleton. Nature Materials. 2006;5(8):636-40.

[3] Bursac P, Lenormand G, Fabry B, Oliver M, Weitz DA, Viasnoff V, et al. Cytoskeletal remodelling and slow dynamics in the living cell. Nature Materials. 2005;4(7):557-61.

[4] Fabry B, Maksym GN, Butler JP, Glogauer M, Navajas D, Fredberg JJ. Scaling the microrheology of living cells. Phys Rev Lett. 2001;87(14):148102.

[5] Fabry B, Maksym GN, Butler JP, Glogauer M, Navajas D, Taback NA, et al. Time scale and other invariants of integrative mechanical behavior in living cells. Physical Review E. 2003;68(4):041914.

[6] Rahatekar SS, Koziol KK, Kline SR, Hobbie EK, Gilman JW, Windle AH. Length-Dependent Mechanics of Carbon-Nanotube Networks. Advanced Materials. 2009;21(8):874-8.

[7] Ureña-Benavides EE, Kayatin MJ, Davis VA. Dispersion and Rheology of Multiwalled Carbon Nanotubes in Unsaturated Polyester Resin. Macromolecules. 2013;46(4):1642-50.

[8] Chen DTN, Chen K, Hough LA, Islam MF, Yodh AG. Rheology of Carbon Nanotube Networks During Gelation. Macromolecules. 2010;43(4):2048-53.